2026 IEEE/SICE International Symposium on System Integration (SII)
January 11-14, 2026. Cancún, México

Series Elastic Actuated Needle Valve and Sealing Equilibrium Flow Rate Models for Precise Position Control in Single-Acting Water-Hydraulic Actuators

Shuto Yoshimura[1], Yuki Nakamura[2], Tomoyuki Noda[3], and Yoshihito Nakata[4]

***Abstract*— Water hydraulics offer low viscosity, high-pressure capability, and environmental compatibility, making them ideal for teleoperated systems in extreme environments. However, achieving stable low-flow control and reliable sealing remains a key challenge owing to the complexity of current valve designs, and their limited precision at low-flow rates. To address this issue, we developed a compact needle valve—called Series Elastic Actuated Needle Valve (SEANV)—which incorporates a series elastic element, along with a sealing equilibrium model to predict its sealing behavior. Preliminary experiments using a single-acting actuator confirmed improved position tracking; however, these did not quantitatively characterize the flow control performance. Therefore, we conducted a detailed experimental evaluation of the flow and sealing characteristics of SEANV under various single-acting actuator conditions. The results demonstrate the enhanced low-flow resolution, achieving an RMSE of 0.516×10^3 $\mathrm{mm^3/s}$, and robust sealing performance, with leakage maintained within ± 50 $\mathrm{mm^3/s}$, thereby validating the applicability of the proposed model to compact water-hydraulic systems.**

I. INTRODUCTION

In extreme environments, electronic devices frequently suffer reliability degradation, making fluid-powered teleoperated robots a promising alternative. Among fluid power sources, water hydraulics stands out for its low viscosity relative to oil hydraulics, high-pressure capability exceeding that of pneumatics, and reduced environmental impact [1], [2].

Achieving precise control in water-hydraulic system requires stable regulation of low-flow rates and robust sealing. However, existing water-hydraulic valves are typically designed for high flow rates, primarily targeting large-scale machinery as alternatives to conventional oil-hydraulic systems (i.e., on the order of tens to hundreds of L/min [3]–[10]), which hampers their performance at low flows. In this study, we define *low-flow* as a rate below 1 $\mathrm{L/min}$; in particular, we focus on rates within 10×10^3 $\mathrm{mm^3/s}$ (0.60 $\mathrm{L/min}$). However, under low-flow conditions, pressure fluctuations, leakage paths, and small valve-opening variations have a significant impact on flow characteristics of such valves. Ensuring adequate sealing performance often necessitates large servo motors to control the valve, which limits system miniaturization. For instance, previous studies on poppet valves did not achieve precise low-flow control and remain unsuitable for compact, precision hydraulic actuators [3]–[6]. Though needle valves are commonly used in manually operated hand valves, they require high actuation and exhibit large variations in contact force near the sealing region, this behavior demands high-precision displacement control, rendering traditional needle valves impractical for compact servo-driven systems.

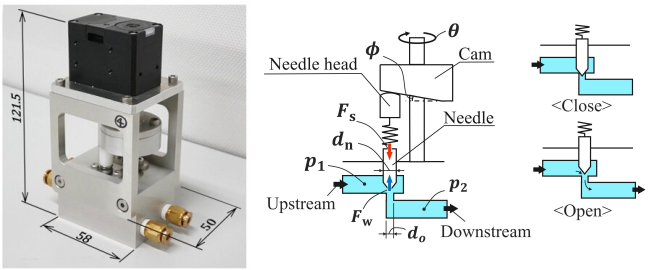

(a) Prototype (b) Design concept

Fig. 1: Picture and schematic diagram of SEANV

To overcome these limitations, we developed the Series Elastic Actuated Needle Valve (SEANV), a compact needle valve that incorporates a series elastic element; it regulated the pressing force rather than the displacement [11]. This design enables flow control based on the force equilibrium between hydraulic pressure and the elastic element. We also proposed a sealing equilibrium model to estimate the contact force required for sealing and a flow-rate model to characterize the low-flow behavior. Using the SEANV and these analytical models, we initially conducted position-control experiments with a single-acting water-hydraulic actuator, confirming improved tracking accuracy within ± 0.5 mm. However, the experiments did not quantitatively assess the flow-tracking performance and deviations between target and actual flow rates, leaving the valve's low-flow capability

*This work was partially supported by JSPS KAKENHI (Grant Number 24K21325), and conducted in collaboration with Chugai Technos Corporation.

[1]Shuto Yoshimura and [4]Yoshihiro Nakata are with the Department of Mechanical and Intelligent Systems Engineering, Graduate School of Informatics and Engineering, The University of Electro-Communications, 1-5-1 Chofugaoka, Chofu, Tokyo, 182-8585, Japan [4]ynakata@uec.ac.jp

[2]Yuki Nakamura is with Chugai Technos Corporation, 9-12 Yokokawa Shinmachi, Nishi-ku, Hiroshima City, 733-0013, Japan, and with the Department of Mechanical and Intelligent Systems Engineering, Graduate School of Informatics and Engineering, The University of Electro-Communications, 1-5-1 Chofugaoka, Chofu, Tokyo, 182-8585, Japan yuki.nakamura@chugai-tec.co.jp

[3]Tomoyuki Noda is with the Department of Brain Robot Interface, ATR Computational Neuroscience Laboratories, 2-2-2 Hikaridai Seika-cho, Soraku-gun, Kyoto, 619-0288, Japan, and with the Department of Mechanical and Intelligent Systems Engineering, Graduate School of Informatics and Engineering, The University of Electro-Communications, 1-5-1 Chofugaoka, Chofu, Tokyo, 182-8585, Japan. t_noda@atr.jp

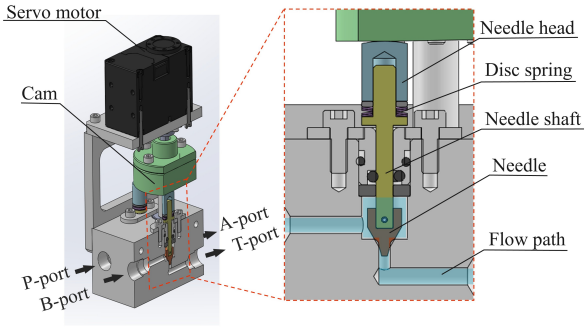

Fig. 2: Structure of SEANV

TABLE I: VALVE COMPARISON

Kind	Sealing	Low-flow	Simplified flow path
Spool valve [7]–[10]	–	–	–
Poppet valve [3]–[6]	✓	–	–
SEANV (This study)	✓	✓	✓

insufficiently verified.

Therefore, in this study, we further analyzed data from previous control experiments using a single-acting actuator equipped with the proposed valve to quantitatively evaluate its performance in the low-flow region. The analyses confirmed the low-flow control and sealing performance of the proposed valve.

The main contributions of this study are as follows:

1) A novel valve for water-hydraulic actuators, which achieves both low-flow control and sealing performance, and a model that describes its operating characteristics are presented.
2) The sealing performance and low-flow control capability of SEANV are experimentally validated and quantitatively evaluated based on the sealing equilibrium and flow-rate models by conducting position-control tests under varying conditions.

II. SERIES ELASTIC ACTUATED NEEDLE VALVE

This section presents the design concept and basic structure of the SEANV, followed by the derivation of the sealing equilibrium and flow-rate models. We also compare its characteristics with those of previously developed valves. A prototype of the SEANV is shown in Fig. 1(a).

A. Related Works and Design Concept

In water-hydraulic robots for extreme environments, the key requirements are: (1) high sealing performance, (2) precise low-flow control, (3) a wide operating pressure range, and (4) a compact, simplified structure. Conventional water-hydraulic spool and poppet valves struggle to simultaneously satisfy all these requirements owing to internal leakage and complex flow paths. Previous research focused on these two valve types. Table I summarizes their characteristics. Spool valves achieve proportional pressure control via spool displacement, but the low viscosity of water makes adequate sealing difficult [12]. NACOL Co., Ltd. developed a spool-type proportional control valve that mitigates leakage by optimizing the spool geometry and material, achieving ± 7 L/min flow control [13]. Nevertheless, some spool valves still exhibit internal leakage ≥ 0.3 L/min, limiting on miniaturization and precise low-flow control [7], [9]. Furthermore, previous studies have not sufficiently addressed low-flow rate resolution, leakage characteristics, or the application of such valves to actuator position.

To overcome these challenges, we propose a compact needle valve with a series elastic element. Despite its simple structure, this design regulates the pressing force of the needle via an elastic element, delivering both high sealing performance and fine control in the low-flow regime. This approach enables miniaturization and precise control in low-flow ranges that conventional valves cannot achieve.

B. Basic Structure

Fig. 1(b) illustrates the design concept of SEANV. A disc spring is placed in series with the needle, and the opening is adjusted via a cam mechanism. The elastic element maintains appropriate contact force when pressing the needle against the seat for robust sealing and precise low-flow control. Under excessive pressure, the elastic deformation of the spring provides a controlled drain path, enhancing system compliance.

The cam mechanism adjusts the needle opening by transforming the motion of a servo motor from rotational to linear. We employed the XM430-W350 (Robotis), with a resolution of 0.0879 deg/pulse, to achieve precise positioning of the cam. The drain-side cross section is shown in Fig. 2; the supply side is configured similarly. Rotating the cam simultaneously adjusts the supply and drain valve openings. An elastic structure, consisting of disc springs, is placed between the head and body of the needle to maintain sufficient contact force and ensure sealing performance. Four disc springs are installed on each needle shaft to ensure sufficient contact force. While disc-spring stiffness depends on stacking configuration [14], they were arranged to yield a stiffness equivalent to that of a single disc spring. The needle head and needle were fabricated from polyoxymethylene, the cam from duralumin, and the remaining components from aluminum alloy, stainless steel, or brass.

C. Sealing Equilibrium Model

The SEANV achieves sealing by pressing the needle against the seat through an elastic element. The required spring displacement for sealing follows from the equilibrium between the fluid force lifting the needle and the elastic force pressing it, allowing us to model the sealing force.

Table II defines the parameters used in the model. Based on Fig. 1(b), the fluid force on the needle is

$$F_w = \frac{\pi}{4}(d_{\mathrm{n}}^2 p_1 - d_{\mathrm{o}}^2 \Delta p), \tag{1}$$

where $\Delta p = p_1 - p_2 \geq 0$. Assuming a linear spring constant k, the disc-spring contact force is

$$F_{\mathrm{s}} = k(z_0 - z_{\mathrm{c}}). \tag{2}$$

TABLE II: SUMMARY OF SEANV PARAMETERS

Symbol	Definition	Value	Unit
d_n	Diameter of the needle shaft	3	mm
d_o	Seat diameter	2.27	mm
r	Radius of the spherical needle head	20	mm
ϕ	Slope angle of the cam	1	deg
θ	Cam rotation angle	-90–90	deg
k	Spring constant of the disc spring	544	N/mm
z_p	Intersection between the cam slope and z-axis	51.848	mm
z_c0	Height of the needle head's spherical surface center for $\theta = 0$	31.848	mm
z_0	Initial deflection of the disc spring	Fitted	mm
z_c	Spring displacement	Variable	mm
p_1	Upstream pressure	Variable	MPa
p_2	Downstream pressure	Variable	MPa
Δp	Pressure difference between ports	Variable	MPa

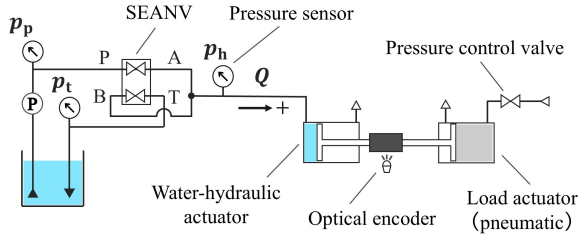

Fig. 3: Single-acting water-hydraulic actuator control system

Sealing occurs when $F_\mathrm{s} \geq F_\mathrm{w}$, i.e., the needle contacts the seat and closes the flow path. Equating F_s and F_w yields the sealing threshold displacement:

$$z_\mathrm{c} = z_0 - \frac{\pi}{4k}(d_\mathrm{n}^2 p_1 - d_\mathrm{o}^2 \Delta p). \tag{3}$$

Next, we relate the disc-spring displacement z_c to the cam rotation angle θ in a Cartesian coordinate system. Let $(x_\mathrm{c}, y_\mathrm{c}, z_\mathrm{c})$ denote the center of the spherical surface of the needle head. Then, the vertical position of the needle head is:

$$\begin{aligned} z_\mathrm{c} =& (x_\mathrm{c} - r\sin\phi\cos\theta)\tan\phi\cos\theta \\ &- (y_\mathrm{c} - r\tan\phi\cos\theta)\tan\phi\sin\theta \\ &- (z_\mathrm{p} - r\cos\phi) - z_\mathrm{c0}. \end{aligned} \tag{4}$$

Combining (3) and (4) gives the relationship between the pressure difference Δp at the sealing threshold and the sealing threshold angle θ_d. Because inverting (4) analytically is difficult, we use an interpolation function based on these equations, implemented with `scipy.interpolate.interp1d` [15], for control and data analysis.

D. Pressure–Flow Relationship

In the prototype SEANV, we investigate how the pressure difference between ports affects the sealing performance and flow rate. To apply the model derived in Section II-C to position control of a water-hydraulic actuator, we perform parameter identification using experimental data and evaluate applicability of the flow-rate model to the prototype valve.

1) Flow-rate model: When the cam rotation angle exceeds the sealing threshold angle θ_d, the valve flow rate Q can be approximated as a quadratic function of the cam angle: $Q = \alpha(\theta - \theta_\mathrm{d})^2$. Here, the coefficient α [mm^3/(s·deg^2)] represents the flow-rate sensitivity to cam-angle changes. According to the orifice flow-rate model [16], α is proportional to the square root of the pressure difference: $\alpha = C\sqrt{\Delta p}$, where C depends on the orifice cross-sectional area and fluid density. Identifying C from experimental data yields the combined expression:

$$Q = C(\theta - \theta_\mathrm{d})^2\sqrt{\Delta p}. \tag{5}$$

Rearranging (5), the cam rotation angle required to achieve flow rate Q is:

$$\theta = \theta_\mathrm{d} \pm \sqrt{\frac{Q}{C\sqrt{\Delta p}}} \tag{6}$$

where the positive or negative sign denotes the supply or drain side, respectively, resulting in separate parameter sets. The valve opens toward either the drain or supply side, depending on whether $\theta \leq \theta_\mathrm{d}$ or $\theta \geq \theta_\mathrm{d}$, respectively.

2) Parameter identification of the flow-rate model: We investigated the relationships among pressure difference, flow rate, and cam rotation angle through flow-evaluation experiments using the single-acting water-hydraulic actuator test setup shown in Fig. 3. The supply and drain sides were measured separately. Flow rate was calculated from actuator velocity and the pressure-receiving area, using maximum (supply) and minimum (drain) velocities, respectively. To apply a load, we employed a pneumatic load actuator (piston diameter: 32 mm, rod diameter: 12 mm, stroke: 100 mm); hereafter, "load" refers to the pneumatic actuator pressure. In Section II-D.1, p_1 and p_2 correspond to the driving pressure p_p (P-port) and the actuator head-side pressure p_h (A/B-port) on the supply side, and to p_h and atmospheric pressure p_t (T-port) on the drain side.

Fig. 4(a) presents the experimental results, showing that flow rate varies gradually with cam rotation angle. On the drain side, negligible flow occurred when A/B-port pressure was below 1.37 MPaG (gauge pressure). The drain-side flow rate decreased slightly every three measurements, indicating minor temporal changes in flow characteristics.

Based on these measurements, we constructed flow-rate models for control. Observed flow rates of ± 50 mm^3/s—regardless of cam angle—indicated internal leakage; thus, we excluded these leakage data from analysis. For the drain side, when load was ≤ 0.2 MPaG, the absolute flow rate did not exceed 500 mm^3/s, which is significantly lower than that in other conditions. These data were excluded because actuator friction prevented accurate load-flow measurement. We also observed instability and increased fitting error at large cam openings, so we limited the analysis range to -40–10 deg.

Using the filtered data, we fitted a quadratic function mapping cam rotation angle to the flow rate. We modeled the relationship between the sealing threshold angle and pressure difference via interpolation, using z_0 as a fitting parameter (Fig. 4(b)). Finally, we identified the optimal coefficient C, relating the quadratic coefficient α to $\sqrt{\Delta p}$, and constructed the flow-rate model using the interpolation functions and sensitivity model. The fitting parameters were

- Supply side: $z_0 = -0.155$, $C = 17.435$
- Drain side: $z_0 = -0.026$, $C = -22.636$

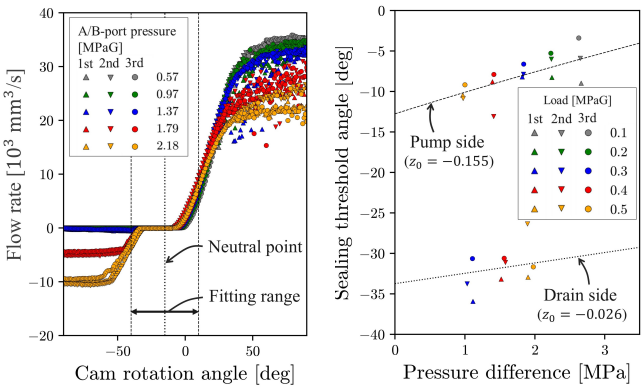

(a) Flow rates (b) Sealing threshold angle

Fig. 4: Flow characterization results of SEANV

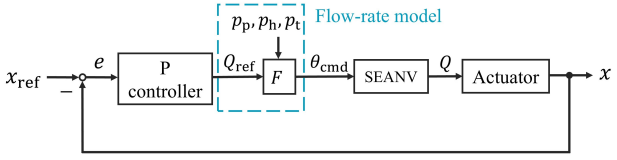

(a) With flow rate model (Proposed)

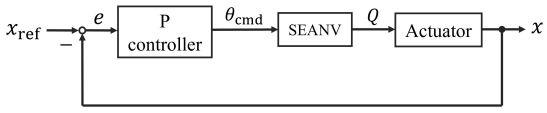

(b) Without flow rate model (conventional P control)

Fig. 5: Block diagram of the position control

III. Experimental Verification

In this section, we quantitatively evaluate the SEANV structure and the validity of its sealing equilibrium and flow-rate models through position-control experiments on a water-hydraulic actuator using the prototype SEANV (Fig. 1(a)).

A. Experimental Setup

The water-hydraulic actuator control system shown in Fig. 3 was used for position control. The driving pressure was set to $p_{\mathrm{p}} = 3.3$ MPaG. To simulate a remote setup, 20 m nylon tubes (inner diameter 2.5 mm, N2-4-4 $\times$ 2.5, Nitta Corporation) connected the actuator (piston diameter 16 mm, rod diameter 8 mm, stroke 75 mm) to pressure sensor (PSE577-02, SMC Corporation) for measuring the A/B-port pressure p_{h} of the SEANV.

Fig. 5 shows a block diagram of the control system. We use a simple P controller, where the error e [mm] between the reference position x_{ref} [mm] and measured position x [mm] from an optical encoder (AEDR-871x, Broadcom Inc.). The control frequency is 100 Hz. In the proposed method (Fig. 5(a)), controller output is interpreted as the target flow rate Q_{ref} [mm^3/s]. We substitute Q_{ref} into the flow-rate model F defined in (6) to compute the target cam angle θ_{cmd} [deg] for the servomotor. In contrast, the conventional P-control approach (Fig. 5(b)) uses no prior knowledge of valve flow characteristics, interpreting the controller output directly as the target cam angle. In both cases, the cam angle command θ_{cmd} was constrained within the model's valid range, i.e., $-40 \leq \theta_{\mathrm{cmd}} \leq 10$.

B. Experimental Conditions

Position-control experiments were conducted under varying loads applied by an external pneumatic actuator. We evaluated tracking performance of actual flow versus target flow in the single-acting water-hydraulic actuator. Measurements were performed both with and without incorporating the flow characteristics of the valve into the control strategy, enabling comparative analysis. We used measurement data from our previous study [11]. In all conditions, the proportional gain K_{p} was determined by the ultimate sensitivity method, with 30 % of the resulting value adopted: $K_{\mathrm{p}} = 15$ without the model and $K_{\mathrm{p}} = 480$ with the model. We evaluated position-control performance differences with and without the flow-rate model.

We defined convergence as a position deviation within ± 0.5 mm. After convergence, the SEANV was held at a fixed cam angle: neutral position (-15 deg) when flow characteristics were not considered, and at 3 deg below the sealing threshold on the supply side when they were. The target position of the actuator was 0 mm for the first 5 s, then changed every 15 s in the sequence: 30, 15, 30, 33, 30, and 0 mm. The load actuator pressure alternated between 0.35 and 0.45 MPaG every 15 s.

C. Results

1) Position control experiment for SEANV flow evaluation: Fig. 6 compares position-control under load variation without (Fig. 6(a)) and with (Fig. 6(b)) flow characteristic compensation. Without compensation, overshoot increased, indicating a relatively high effective gain. When the valve opening remained in the sealing region around the target position, the actuator failed to respond to load variations. Small position errors did not generate sufficient flow for correction, impeding precise adjustment. In contrast, with flow-characteristic compensation, the valve opening was precisely modulated according to position error, allowing flow rate to decrease gradually as the error diminished and enabling smooth trajectory tracking.

2) Control characteristics at low-flow rates: The tracking performance and deviation between actual and target flow rates during position control were evaluated based on the results in Fig. 6(b). Fig. 7(a) shows time histories of target and actual flow rates. The actual flow rate exhibited a delay of approximately 0.25 s relative to the target. Of this delay, 0.1 s can be attributed to servo-response lag, whereas the remaining delay is likely due to unmodeled dynamics such as tubing expansion and fluid viscous resistance [17]. A quantitative analysis of this delay will be conducted in future work.

To align the flows, we shifted the actual flow data forward by 0.25 s. Fig. 7(b) visualizes the deviation between target

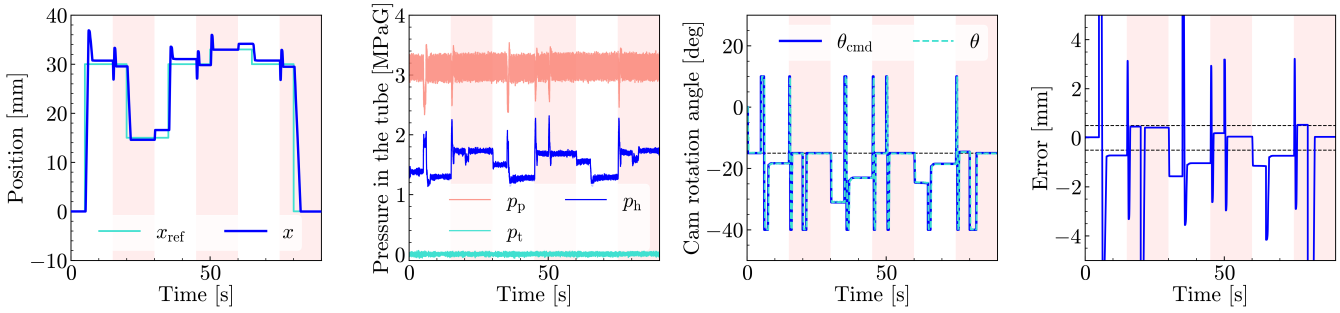

(a) Without flow rate model

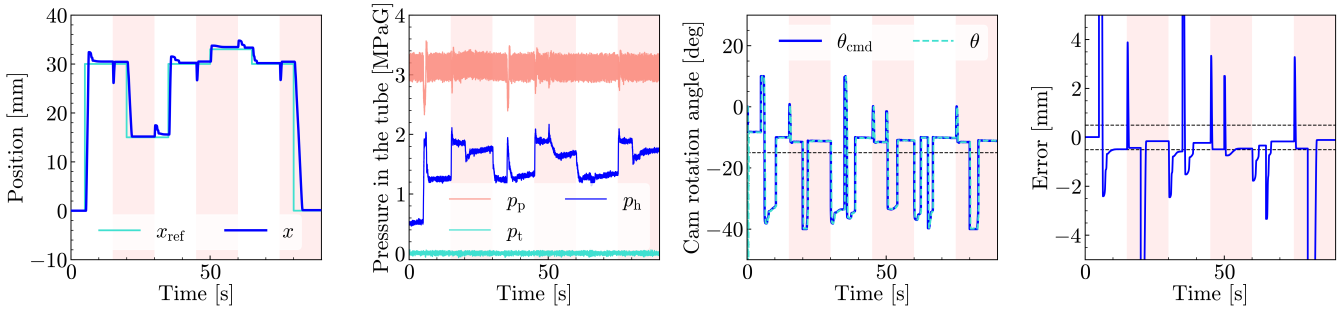

(b) With flow rate model

Fig. 6: Load variation experiment results for single acting system. Shaded regions correspond to a 0.45 MPaG load. From left: Target and actual position, Measured pressures, Cam rotation angles (black dashed: neutral), Error.

and actual flows. We observed instances where actual flow changed despite a constant target, due to the stepwise target adjustments and load variations versus continuous actual flow changes after valve opening. The actual flow Q tracked the target within -2.5×10^3 mm^3/s to 8×10^3 mm^3/s, with an RMSE of 0.516×10^3 mm^3/s in this range. Outside this range, constant flow was maintained by limiting the cam angle. The supply side exhibited larger fluctuations relative to the drain side, likely due to greater supply-side pressure variations from pump pulsations and fluid inertia. The actual flow tended to converge to 0 mm^3/s when the target flow was $\pm 2 \times 10^3$ mm^3/s. However, on the supply side, actual flow occasionally rose to 3×10^3 mm^3/s for a target flow of 1×10^3 mm^3/s.

IV. DISCUSSION

The position-control experiments confirmed that the SEANV and its accompanying model deliver reliable control performance in the low-flow region, which has been challenging for conventional water-hydraulic valves designed for high flow rates. Although a delay of approximately 0.25 s was observed in the flow-rate control, the intended applications of this system in extreme environments prioritize stable low-speed operation and precise positioning over rapid response. Therefore, a delay of this magnitude is not expected to impair practical performance. Separate flow-evaluation tests demonstrated high sealing performance, with a measured leakage rate of ± 50 mm^3/s. These results indicate that the proposed valve can enable high-precision position control in compact robotic systems.

Incorporating the sealing equilibrium model into the control strategy allows it to account for the sealing threshold angle, enabling the actuator to operate near the angle within the convergence region and improving responsiveness. Additionally, the elastic structure of the SEANV, combined with the equilibrium model, could facilitate variable control of secondary pressure upper limits under overload conditions.

Despite these advantages, the SEANV flow characteristics exhibited temporal variations, including a significant drain-side flow rate decrease with repeated use (Fig. 4(a)). Consequently, in Section III-C.2, instances occurred where the actual flow rate dropped to 0 mm^3/s for a target flow of $\pm 2 \times 10^3$ mm^3/s. Although the cam mechanism is designed for a positive sealing threshold angle on the supply side, experimental results placed this threshold in the negative region. Possible causes include POM needle deformation from swelling, creeping, or cavitation effects. Moreover, assuming a fixed spring constant for the disc spring and its potential plastic deformation may contribute to model error. Additionally, the present study modeled flow behavior in the low-flow region using a quadratic approximation. Such formulation imposes a fundamental limitation to the model because it cannot accurately capture behavior beyond the inflection point.

The flow characteristics of the SEANV were estimated indirectly from actuator velocity to emulate actual control conditions. However, nonlinear actuator friction introduces uncertainty in flow estimation, especially on the drain side where the actuator often remained stationary despite valve

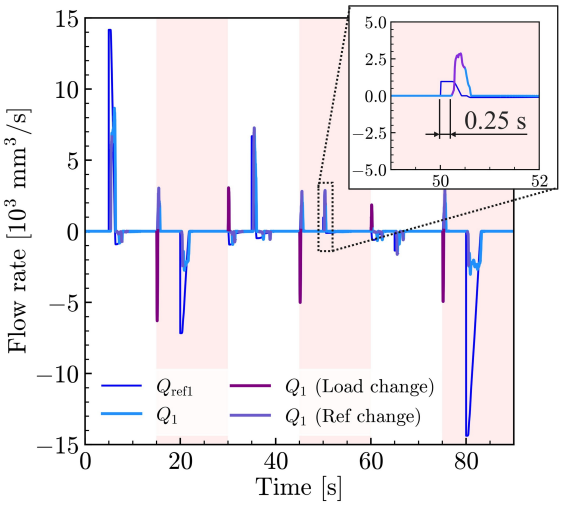

(a) Target and actual flow rates over time

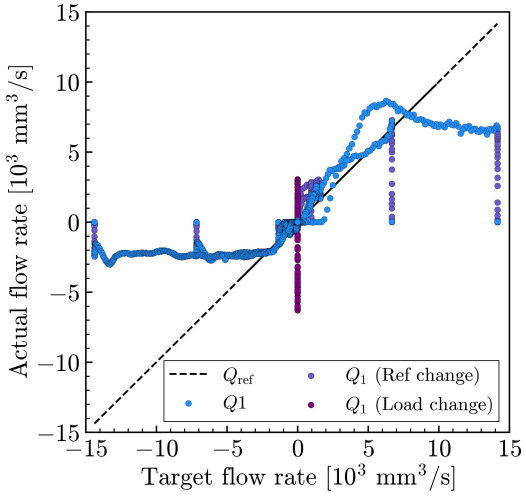

(b) Actual vs. target flow rate (with a 0.25 s delay compensation). Q_{ref} solid line: fitting range.

Fig. 7: Flow control performance during position control. Shaded regions correspond to a 0.45 MPaG load. Highlight 0.25 s after flow change due to load and reference changes.

opening and pressure variations, resulting in significant experimental variability. Furthermore, as evaluations used a single-acting actuator over a limited number of cycles, the long-term stability and durability of the SEANV, including its sealing performance due to material deformation, remain unverified. Future work should validate the valve and model under double-acting configurations and extended operational periods.

V. CONCLUSION

This study presented a novel valve for water-hydraulic actuators, Series Elastic Actuated Needle Valve (SEANV), as well as a model describing its operating characteristics. The valve, which incorporates an elastic element placed in series with the needle, aimed to achieve high-precision position control in water-hydraulic robots under extreme environments. Position-control experiments on a single-acting water-hydraulic actuator equipped with the SEANV quantitatively evaluated the flow characteristics of proposed structure and the model accuracy. The results demonstrated that, despite its compact and simple flow path structure, the SEANV achieves high sealing performance and precise low-flow control, and that the proposed model supports high-precision position control.

REFERENCES

[1] S.-H. Hyon and K. Akama, "Air-hydraulic servo booster toward submersible water-driven robots," *IEEE Robotics and Automation Letters*, vol. 6, no. 2, pp. 1966–1972, 2021.

[2] Y. Nakamura, T. Noda, and Y. Nakata, "Remote controlled water hydraulic robot (in Japanese)," *Journal of the Robotics Society of Japan*, vol. 43, no. 3, pp. 267–270, 2025.

[3] S. Park and T. Kitagawa, "Analysis of main valve dynamics of a two-stage high-speed solenoid valve for water hydraulics using hils (in Japanese)," *Transactions of the Japan Fluid Power System Society*, vol. 36, no. 3, pp. 66–73, 2005.

[4] S.-H. Park, "Design and performance characteristic analysis of servo valve-type water hydraulic poppet valve," *Journal of mechanical science and technology*, vol. 23, pp. 2468–2478, 2009.

[5] M. Han, Y. Liu, D. Wu, H. Tan, and C. Li, "Numerical analysis and optimisation of the flow forces in a water hydraulic proportional cartridge valve for injection system," *IEEE Access*, vol. 6, pp. 10 392–10 401, 2018.

[6] Y. Liao, W. Zhao, J. Feng, and Z. Lian, "Optimization of the control performance of a novel 3/2 water proportional directional valve with a special position following servo mechanism," *IEEE/ASME Transactions on Mechatronics*, vol. 29, no. 5, pp. 3391–3400, 2024.

[7] T. Takahashi, C. Yamashina, and S. Miyakawa, "Development of water hydraulic proportional control valve," in *Proceedings of the JFPS international symposium on fluid power*, vol. 1999, no. 4. The Japan Fluid Power System Society, 1999, pp. 549–554.

[8] R. Amirante, E. Distaso, and P. Tamburrano, "Experimental and numerical analysis of cavitation in hydraulic proportional directional valves," *Energy Conversion and Management*, vol. 87, pp. 208–219, 2014.

[9] K. Suzuki, S. Akazawa, and Y. Nakao, "Development of cam-drive type proportional valve for water hydraulics," *International Journal of Automation Technology*, vol. 6, no. 4, pp. 450–456, 2012.

[10] H. Wang, C. Cao, J. Zhao, Y. Wang, and H. Zhang, "Design and dynamic characteristics measurement of a water hydraulic proportional flow valve with a discrete pilot stage," *IEEE Transactions on Instrumentation and Measurement*, 2025.

[11] S. Yoshimura, Y. Nakamura, T. Noda, and Y. Nakata, "Position control of a water hydraulic actuator using a series elastic actuated needle valve (in Japanese)," Oral presentation, 43rd Annual Conference of the Robotics Society of Japan, 2025.

[12] S. Park and T. Kitagawa, "Development and fundamental characteristics analysis of a proportional poppet valve for water hydraulics (in Japanese)," *Transactions of the Japan Fluid Power System Society*, vol. 36, no. 2, pp. 51–58, 2005.

[13] H. Shimoyama, T. Makita, and K. Sugimura, "Development of hydraulic devices for robot actuation (in Japanese)," *Journal of the Robotics Society of Japan*, vol. 43, no. 3, pp. 275–278, 2025.

[14] Y. Chen, C. Chiu, and Y. Cheng, "Dynamic analysis of disc spring effects on the contact pressure of the collet–spindle interface in a high-speed spindle system," *Proc. Inst. Mech. Eng., Part C: J. Mech. Eng. Sci.*, vol. 223, no. 5, pp. 1191–1201, 2009.

[15] P. Virtanen, R. Gommers, T. E. Oliphant, M. Haberland, T. Reddy, D. Cournapeau, E. Burovski, P. Peterson, W. Weckesser, J. Bright, *et al.*, "Scipy 1.0: fundamental algorithms for scientific computing in python," *Nature Methods*, vol. 17, no. 3, pp. 261–272, 2020.

[16] L. Lei, Z. Desheng, and Z. Jiyun, "Design and research for the water low-pressure large-flow pilot-operated solenoid valve," *Strojniški vestnik-Journal of Mechanical Engineering*, vol. 60, no. 10, pp. 665–674, 2014.

[17] C. Véronneau, J.-P. L. Bigué, A. Lussier-Desbiens, and J.-S. Plante, "A high-bandwidth back-drivable hydrostatic power distribution system for exoskeletons based on magnetorheological clutches," *IEEE Robotics and Automation Letters*, vol. 3, no. 3, pp. 2592–2599, 2018.